

CMB lensing reconstruction in the presence of diffuse polarized foregrounds

Y. Fantaye,^a C. Baccigalupi,^{a,b} S. M. Leach^a and A. P. S. Yadav^c

^aSISSA, Astrophysics Sector, via Bonomea 265, Trieste 34136, Italy

^bINFN, Sezione di Trieste, Via Valerio 2, I-34151 Trieste, Italy

^cSchool of Natural Sciences, Institute for Advanced Study, Einstein Drive, Princeton, NJ 08540

E-mail: fantaye@sissa.it

Abstract. The measurement and characterization of the lensing of the cosmic microwave background (CMB) is a key goal of the current and next generation of CMB experiments. We perform a case study of a three-channel balloon-borne CMB experiment observing the sky at $(l,b)=(250^\circ, -38^\circ)$ and attaining a sensitivity of $5.25 \mu\text{K-arcmin}$ with $8'$ angular resolution at 150 GHz, in order to assess whether the effect of polarized Galactic dust is expected to be a significant contaminant to the lensing signal reconstructed using the EB quadratic estimator. We find that for our assumed dust model, polarization fractions as low as a few percent may lead to a significant dust bias to the lensing convergence power spectrum. We investigate a parametric component separation method, proposed by Stompor et al. (2009), for mitigating the effect of this dust bias, based on a ‘profile likelihood’ technique for estimating the dust spectral index. We find a dust contrast regime in which the accuracy of the profile likelihood spectral index estimate breaks down, and in which external information on the dust frequency scaling is needed. We propose a criterion for putting a requirement on the accuracy with which the dust spectral index must be estimated or constrained, and demonstrate that if this requirement is met, then the dust bias can be removed.

Contents

1	Introduction	1
2	Data analysis techniques	2
2.1	CMB lensing and the quadratic estimator	2
2.2	Foreground spectral index estimation and cleaning	4
3	CMB and polarized dust simulations	5
4	Results	8
4.1	Foreground-free case	8
4.2	Dust polarization bias at 150 GHz	9
4.3	Debiasing the effect of dust via foreground cleaning	11
5	Conclusions	14

1 Introduction

The measurement and characterization of the weak lensing of the cosmic microwave background (CMB) by the large-scale structure distribution is a promising and active field of research in observational cosmology (for a review of the physics of CMB weak lensing, see [1]). Measurements of this signal can break fundamental degeneracies that afflict the cosmological interpretation of measurements of the CMB power spectrum [2] as well as help to improve the constraints on the cosmological parameters [3, 4]. As a result, a number of ongoing and planned experiments are targeting the weak lensing signal as one of their primary science goals.

The CMB weak lensing signal was first detected by [5] who cross correlated data from the Wilkinson Microwave Anisotropy Probe (WMAP) satellite with a tracer of large-scale structure in the form of the NRAO VLA sky survey. Since then observational progress has been rapid: the Atacama Cosmology Telescope (ACT) collaboration made the first detection of weak lensing signal using CMB data alone [6] and the South Pole Telescope (SPT) collaboration have followed with a detection at higher significance [7] as well as detecting the correlation of the weak lensing ‘convergence’ and large-scale structure tracers from the Wide-field Infrared Survey Explorer and Spitzer/IRAC [8]. First applications of the weak lensing signal measurements have been to provide corroborating evidence for the cosmological constant from CMB data alone [9] and to improve constraints on the dark energy equation of state [7]. In the future, improved cosmological constraints are expected from the full SPT and ACT surveys, and especially from *Planck* which is poised to significantly advance lensing studies [10, 11].

The most widely adopted technique for extracting the lensing signal, also implemented in this investigation, is the ‘quadratic estimator’ suggested by [12] which is a near optimal framework for reconstructing the lensing field using a quadratic combination of an appropriately filtered CMB temperature and/or polarization map and its gradient. The subsequent estimation of the power spectrum of the lensing field is met by a variety of real world complications. These include intrinsic biases of the quadratic estimator which must be modeled

and subtracted [11, 13], and any effect that breaks the statistical isotropy of data including anisotropic noise [14] and the effect of instrumental systematics [15, 16].

Astrophysical foregrounds represent another source of contamination to the lensing signal for which there have been several simulation studies assessing their possible impact and suggesting mitigation strategies. [17] performed simulations of the kinetic Sunyaev-Zeldovich (SZ) effect and pointed out that this non-Gaussian effect correlated with the lensing signal, with a spectrum indistinguishable from CMB anisotropies, could potentially bias the lensing reconstruction. They proposed masking CMB maps around the location of clusters detected via the thermal SZ effect as a potential strategy for mitigating kSZ biases, a procedure subsequently adopted by the SPT team [7]. [18] made calculation of the lensing biases induced by polarized extragalactic radio point sources, concluding that the effect of these source could be mitigated via source detection/masking, and that these sources ought not pose a significant challenge to a future CMB polarization satellite. [10] studied the impact of diffuse and extragalactic foregrounds on a *Planck*-like simulations and proposed a multi-frequency masking and ‘in-painting’ technique for measuring the lensing signal.

To date there has been no specific study on the possible impact of Galactic polarized dust emission on the detection of the lensing signal. We believe that it is important to make such an assessment given the fact that several ongoing ground-based and balloon-borne CMB polarization experiments including ACTPol [19], SPTPol [20], EBEX [21] and POLARBEAR [22] are targeting the lensing signal in the near future, using measurements of CMB polarization in the frequency range 90–410 GHz. In particular we will focus on performing a case study of an EBEX-like experimental configuration which, owing to observing constraints on balloon-borne telescopes flying from Antarctica, will most likely survey a region of sky where Galactic foregrounds in the form of polarized dust emission may be significant compared to the lensing signal. We aim to develop methods for numerically investigating the extent to which this experiment can expect to be challenged by diffuse polarized dust emission, and to investigate possible dust mitigation strategies.

This study is set out as follows: Section 2 describes the data analysis techniques that we have implemented; Section 3 describes the CMB and dust polarization simulations that we have performed; Section 4 describes our findings and results, and Section 5 contains our conclusions.

2 Data analysis techniques

In this section we review the formalism of the two analysis techniques that we have implemented and investigated in our lensing estimation pipeline. These are the quadratic estimator [12] for estimating the CMB lensing signal, and the multi-frequency analysis technique of [23] for estimating the foreground spectral index and performing separation of the CMB component.

2.1 CMB lensing and the quadratic estimator

CMB photons from the last scattering surface are deflected according to

$$\begin{aligned} \tilde{T}(\hat{\mathbf{n}}) &= T \left[\hat{\mathbf{n}} + \hat{\nabla}\phi(\hat{\mathbf{n}}) \right], \\ (\tilde{Q} + i\tilde{U})(\hat{\mathbf{n}}) &= (Q \pm iU) \left[\hat{\mathbf{n}} + \hat{\nabla}\phi(\hat{\mathbf{n}}) \right], \end{aligned} \tag{2.1}$$

where $\phi(\hat{\mathbf{n}})$ is the projected potential, and $\hat{\mathbf{n}}$ is the direction on the sky [24]. We will adopt the notation convention that lensed quantities are denoted with a tilde and unlensed ones without. In the Born approximation, in which the deflection angles are assumed to be small enough to carry out the projection kernel integration along the line of sight, ϕ is related to the three-dimensional gravitational potential, ψ , by

$$\begin{aligned}\phi(\hat{\mathbf{n}}) &= -2 \int_0^{D_\star} dD \frac{D_\star - D}{DD_\star} \psi(D\hat{\mathbf{n}}, D), \\ &= \int \frac{d^2L}{(2\pi)^2} \phi(\mathbf{L}) e^{i\mathbf{L}\cdot\hat{\mathbf{n}}},\end{aligned}\tag{2.2}$$

where D and D_\star are the comoving angular diameter distances to the lens and the CMB last scattering surface respectively; ϕ is related to the ‘convergence’ κ as $\hat{\nabla}^2\phi = -2\kappa$ [24].

To linear order in ϕ , the changes in the Fourier moments of the temperature and polarization fields due to lensing are [25]

$$\begin{aligned}\delta\tilde{T}(\mathbf{l}) &= \int \frac{d^2l'}{(2\pi)^2} T(\mathbf{l}') W(\mathbf{l}', \mathbf{L}), \\ \delta\tilde{E}(\mathbf{l}) &= \int \frac{d^2l'}{(2\pi)^2} [E(\mathbf{l}') \cos 2\varphi_{l'1} - B(\mathbf{l}') \sin 2\varphi_{l'1}] W(\mathbf{l}', \mathbf{L}), \\ \delta\tilde{B}(\mathbf{l}) &= \int \frac{d^2l'}{(2\pi)^2} [B(\mathbf{l}') \cos 2\varphi_{l'1} + E(\mathbf{l}') \sin 2\varphi_{l'1}] W(\mathbf{l}', \mathbf{L}),\end{aligned}\tag{2.3}$$

where $\varphi_{l'1} \equiv \varphi_{l'} - \varphi_1$, $\mathbf{L} = \mathbf{l} - \mathbf{l}'$, and

$$W(\mathbf{l}, \mathbf{L}) = -[\mathbf{l} \cdot \mathbf{L}] \phi(\mathbf{L}).\tag{2.4}$$

From these equations we note that the effect of lensing is to couple the gradient of the primordial CMB \mathbf{l}' modes to that of the observed \mathbf{l} modes. Furthermore, starting from zero primordial B -modes, $B(\mathbf{l}') = 0$, lensing generates B -mode anisotropies in the observed map.

Quadratic estimators for the convergence: We will assume a CMB map with homogeneous white noise and a Gaussian beam smoothing. The power spectrum of the detector noise is [26]

$$C_l^{N,X} = \sigma_{\text{pix}}^2 \Omega_{\text{pix}},\tag{2.5}$$

where σ_{pix} is the RMS noise per pixel and Ω_{pix} is the solid angle subtended by each pixel. The observed CMB temperature and polarization fields, $X \in [T, E, B]$, and their power spectra, \tilde{C}_ℓ^X , are

$$\begin{aligned}\tilde{X}_1^{\text{obs}} &= \tilde{X}_1 e^{-\frac{1}{2}l^2\sigma_b^2} + N_1^X, \\ \tilde{C}_l^{X,\text{obs}} &= \tilde{C}_l^X e^{-l^2\sigma_b^2} + C_l^{N,X},\end{aligned}\tag{2.6}$$

where N_1^X is the Fourier mode of the detector noise, and σ_b relates to the full-width half-maximum (FWHM) of the telescope beam, θ_{FWHM} , via $\theta_{\text{FWHM}} = \sigma_b \sqrt{8 \ln 2}$.

To extract the lensing information in the observed CMB map we will use the quadratic estimator formalism [12, 27, 28] in the context of the convergence estimators [29, 30]. These estimators are uniquely determined by the requirement that each estimator be unbiased

$\langle \hat{\kappa}^{XY}(\hat{\mathbf{n}}) \rangle = \kappa(\hat{\mathbf{n}})$ over an ensemble average of the CMB temperature and polarization fields X and Y , and the variance of the estimator be minimal,

$$\langle \hat{\kappa}_1^{XY} \hat{\kappa}_1^{*XY} \rangle = (2\pi)^2 \delta^D(\mathbf{l} - \mathbf{l}') (C_l^\kappa + N_l^{\kappa,XY}). \quad (2.7)$$

In real space the convergence estimators are given by [30]

$$\mathbf{G}_{XY}(\hat{\mathbf{n}}) = \int \frac{d^2\mathbf{l}}{(2\pi)^2} i\mathbf{l} \tilde{X}_1^{\text{obs}} \frac{C_l^{XY}}{\tilde{C}_l^{X,\text{obs}}} \begin{Bmatrix} e^{2i\varphi_1} \\ e^{2i\varphi_1} \end{Bmatrix} e^{-\frac{1}{2}l^2\sigma_b^2 + i\mathbf{l}\cdot\hat{\mathbf{n}}}, \quad (2.8)$$

$$W_Y(\hat{\mathbf{n}}) = \int \frac{d^2\mathbf{l}}{(2\pi)^2} \frac{\tilde{Y}_1^{\text{obs}}}{\tilde{C}_l^{Y,\text{obs}}} \begin{Bmatrix} e^{2i\varphi_1} \\ ie^{2i\varphi_1} \end{Bmatrix} e^{-\frac{1}{2}l^2\sigma_b^2 + i\mathbf{l}\cdot\hat{\mathbf{n}}}, \quad (2.9)$$

where φ_1 is the azimuthal angle of the wavevector \mathbf{l} ; the two phase factors in braces are applied when $Y = E, B$ respectively, and is unity when $Y = T$. Also $C_l^{XY} = C_l^{XE}$ for $Y = B$. The construction of these fields incorporate the deconvolution of the beam from the map, hence the beam factors $e^{-\frac{1}{2}l^2\sigma_b^2}$ appearing on both fields.

Given the two filtered fields in Eq. (2.8) and Eq. (2.9), the convergence estimators are then given by

$$\hat{\kappa}_1^{XY} = -\frac{A_l^{XY}}{2} i\mathbf{l} \cdot \int d^2\hat{\mathbf{n}} \text{Re}[\mathbf{G}_{XY}(\hat{\mathbf{n}})W_Y^*(\hat{\mathbf{n}})] e^{-i\mathbf{l}\cdot\hat{\mathbf{n}}}. \quad (2.10)$$

The normalization coefficients, A_l^{XY} , are related to the noise power spectrum, $N_l^{\kappa,XY}$, of the estimators $\hat{\kappa}^{XY}(\hat{\mathbf{n}})$ by $N_l^{\kappa,XY} = l^2 A_l^{XY}/4$, and are calculated as

$$\begin{aligned} \frac{1}{A_l^{XY}} &= \frac{1}{l^2} \int \frac{d^2\mathbf{l}_1}{(2\pi)^2} \frac{(\mathbf{l} \cdot \mathbf{l}_1) C_{l_1}^{XY} f_{\mathbf{l}_1\mathbf{l}_2}^{XY}}{\tilde{C}_{l_1}^{X,\text{obs}} \tilde{C}_{l_2}^{Y,\text{obs}}} \\ &\times \begin{Bmatrix} \cos 2\Delta\varphi \\ \sin 2\Delta\varphi \end{Bmatrix} e^{-l_1^2\sigma_b^2} e^{-l_2^2\sigma_b^2}, \end{aligned} \quad (2.11)$$

with $\mathbf{l} = \mathbf{l}_1 + \mathbf{l}_2$, $\Delta\varphi = \varphi_{\mathbf{l}_1} - \varphi_{\mathbf{l}_2}$, and $\langle X_{\mathbf{l}_1} Y_{\mathbf{l}_2} \rangle = f_{\mathbf{l}_1\mathbf{l}_2}^{XY} \phi_1$, where [28]

$$\begin{aligned} f_{\mathbf{l}_1,\mathbf{l}_2}^{TT} &= (\mathbf{l} \cdot \mathbf{l}_1) C_{l_1}^T + (\mathbf{l} \cdot \mathbf{l}_2) C_{l_2}^T, \\ f_{\mathbf{l}_1,\mathbf{l}_2}^{TE} &= (\mathbf{l} \cdot \mathbf{l}_1) C_{l_1}^C \cos 2\Delta\varphi + (\mathbf{l} \cdot \mathbf{l}_2) C_{l_2}^C, \\ f_{\mathbf{l}_1,\mathbf{l}_2}^{TB} &= (\mathbf{l} \cdot \mathbf{l}_1) C_{l_1}^C \sin 2\Delta\varphi, \\ f_{\mathbf{l}_1,\mathbf{l}_2}^{EE} &= [(\mathbf{l} \cdot \mathbf{l}_1) C_{l_1}^E + (\mathbf{l} \cdot \mathbf{l}_2) C_{l_2}^E] \cos 2\Delta\varphi, \\ f_{\mathbf{l}_1,\mathbf{l}_2}^{EB} &= (\mathbf{l} \cdot \mathbf{l}_1) C_{l_1}^E \sin 2\Delta\varphi. \end{aligned} \quad (2.12)$$

Our code for estimating the convergence using the quadratic estimator formalism is a direct implementation of the above equations, Eq. (2.5)–(2.12).

2.2 Foreground spectral index estimation and cleaning

To perform foreground spectral index estimation and cleaning, we use an implementation of the parametric component separation algorithm proposed by [23] and tested in the context of forecasts for inflationary B -mode detection in [31, 32]. In this framework, the multi-frequency data vector d_p is modeled at each pixel p of the map as

$$d_p = A_p s_p + n_p, \quad (2.13)$$

where $A_p \equiv A_p(\beta)$ is an $N_{\text{freq}} \times N_{\text{comp}}$ ‘mixing’ matrix with N_{spec} free parameters, β , to be estimated, s_p is a vector of N_{comp} component amplitudes also to be estimated, and n_p is the noise. A likelihood for the data is given by

$$-2 \ln \mathcal{L}(s, \beta) = \text{CONST} + (\mathbf{d} - \mathbf{A}\mathbf{s})^t \mathbf{N}^{-1} (\mathbf{d} - \mathbf{A}\mathbf{s}), \quad (2.14)$$

where \mathbf{N}^{-1} is the noise covariance of the map. A key result of [23] is that under the assumption that the spectral index is the same for each pixel, the maximum-likelihood values of the components \mathbf{s} can be found by first locating the values of the spectral parameters β that minimize the value of the ‘profile likelihood’

$$-2 \ln \mathcal{L}_{\text{spec}}(\beta) = \text{CONST} - (\mathbf{A}^t \mathbf{N}^{-1} \mathbf{d})^t (\mathbf{A}^t \mathbf{N}^{-1} \mathbf{A})^{-1} (\mathbf{A}^t \mathbf{N}^{-1} \mathbf{d}), \quad (2.15)$$

which is an expression independent of \mathbf{s} . Once the maximum likelihood spectral parameters, $\hat{\beta}$, have been determined, their values are substituted into the generalized least squares solution of Eq. (2.13), given by

$$\mathbf{s} = (\mathbf{A}^t \mathbf{N}^{-1} \mathbf{A})^{-1} \mathbf{A}^t \mathbf{N}^{-1} \mathbf{d}, \quad (2.16)$$

$$\mathbf{N}_{\mathbf{s}} \equiv (\mathbf{A}^t \mathbf{N}^{-1} \mathbf{A})^{-1}, \quad (2.17)$$

to obtain the estimated component amplitudes, $\hat{\mathbf{s}}$, their noise covariance $\mathbf{N}_{\hat{\mathbf{s}}}$, pixel by pixel.

Insight into the component separation error can be gained using the \mathbf{Z} -matrix formalism derived in [31] where,

$$\mathbf{Z}(\hat{\beta}) = \left(\mathbf{A}^t(\hat{\beta}) \mathbf{N}^{-1} \mathbf{A}(\hat{\beta}) \right)^{-1} \mathbf{A}^t(\hat{\beta}) \mathbf{N}^{-1} \mathbf{A}(\beta_0). \quad (2.18)$$

In our case, this will be a 2×2 matrix corresponding to the two components, CMB and dust. In the limit of $\hat{\beta} = \beta_0$ then \mathbf{Z} is the identity matrix. For the case where the dust spectral index is mis-estimated, then the off-diagonal terms of \mathbf{Z} quantify the fraction of the original component that remains unsubtracted, since

$$\hat{\mathbf{s}}_i = \sum_j^{n_{\text{comp}}} \mathbf{Z}_{ij}(\hat{\beta}) s_j(\beta_0), \quad (2.19)$$

where $\hat{\mathbf{s}}$ are the estimated components.

3 CMB and polarized dust simulations

We simulate CMB polarization and diffuse polarized dust emission on a $13^\circ \times 13^\circ$ patch of sky located at (RA, Dec) = $(75^\circ, -44.5^\circ)$, corresponding to $(l, b) = (250^\circ, -38^\circ)$ in Galactic coordinates. This area of sky is accessible from observing sites both in Antarctica and Chile, has been surveyed by several past ground-based and balloon-borne CMB experiments including Boomerang [33], QUAD [34], ACBAR [35], QUIET [36] and SPT [37], as shown in Figure 1. It is close to the area that will be observed by the balloon-borne CMB experiment EBEX, owing to the fact that is aligned with the anti-sun direction in mid December, soon after the start of the Antarctic long duration balloon flight launch window. Given that the anti-sun direction moves by 1 degree in RA per day in the direction of the Galactic plane, then the sky patch we assume can be considered representative of an early launch scenario

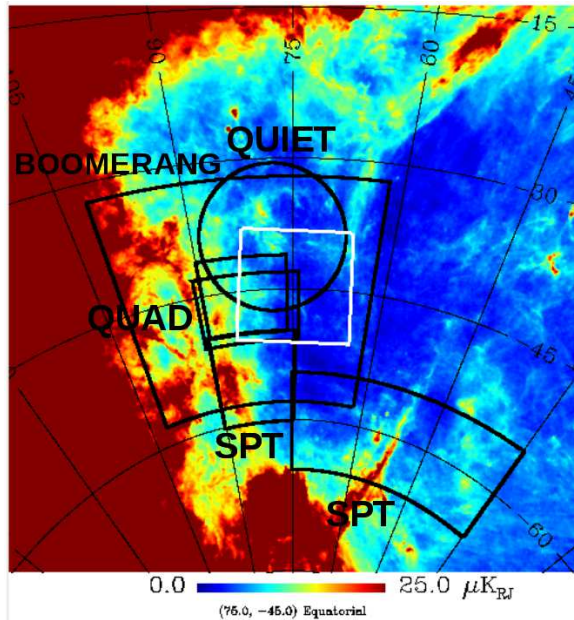


Figure 1. Dust intensity at 150 GHz (thresholded to $25 \mu\text{K}_{\text{RJ}}$). Black outlines show the borders of previous CMB intensity and polarization surveys, while the white outline shows the $13^\circ \times 13^\circ$ patch that we consider in this study.

when the impact of Galactic foregrounds will be at their lowest. Following [32], we assume a three band experimental configuration with channels at 150, 250 and 410 GHz observing to depths of 5.25, 14.0 and $140 \mu\text{K}_{\text{CMB}}\text{-arcmin}$ respectively, each with an angular resolution of $8'$. An advantage of this selection of bands is to minimize the possible impact polarized synchrotron, assumed to be negligible in this study, which may affect ground-based CMB polarization experiments observing at 90 GHz [31].

Our Galactic polarized dust model is the same as the one first described in [31]: dust intensity is given by the model of [38] extrapolated to 410 GHz. Then, to simulate polarized emission, polarization angles are set on large angular scales using the WMAP dust template [39], while on smaller scales, extra Gaussian power is added using the prescription of [40]. The polarization fraction, p , is assumed to be spatially constant, and we investigate three cases of 3.6, 5, and 10%, intended to bracket the average high Galactic latitude dust polarization detected in the WMAP W band [41], and possible higher dust polarization fractions observed by ARCHEOPS at 353 GHz [42]. The dust is scaled from the 410 GHz band to the lower frequency bands assuming a greybody frequency scaling

$$A_{\text{dust}} \propto \frac{\nu^{\beta+1}}{\exp \frac{h\nu}{kT} - 1}, \quad (3.1)$$

with $T = 18\text{K}$ and $\beta = 1.65$, with the dust temperature and spectral index both assumed to be uniform across the patch. The resulting dust polarization simulation at 150 GHz is shown in Figure 2.

For our CMB simulations, we produced two sets of 100 realizations—lensed and unlensed—with $0.76'$ pixel size, assuming the WMAP 7-year best-fit cosmological parameter values [43], and with our fiducial CMB polarization power spectra calculated using CAMB [44].

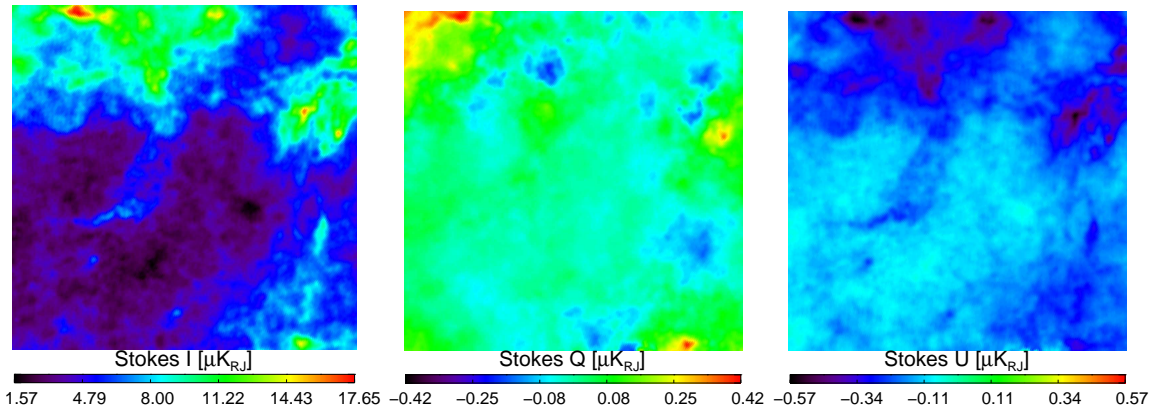


Figure 2. Dust simulation (Stokes I , Q , and U) at 150 GHz, with a polarization fraction $p = 0.036$, on a $13^\circ \times 13^\circ$ patch centred on $(l,b)=(250^\circ, -38^\circ)$.

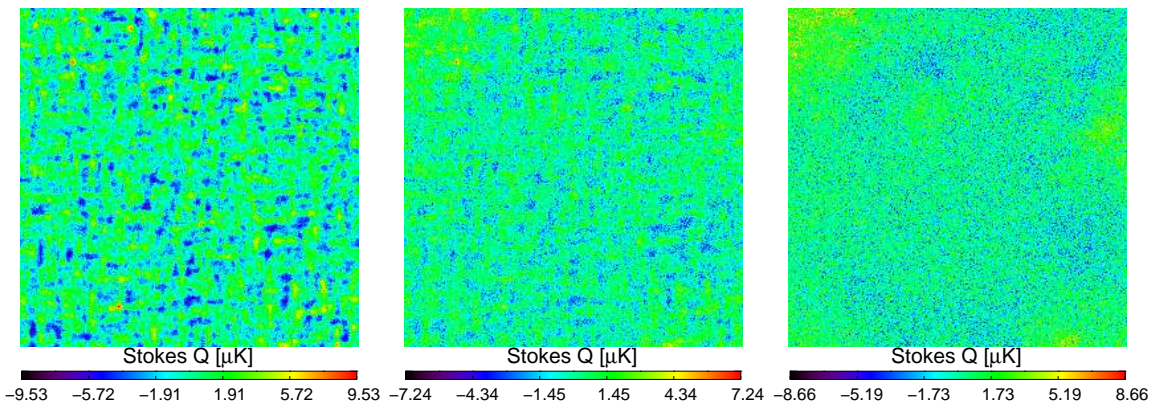


Figure 3. From left to right, we show our CMB+dust+noise simulations at 150, 250 and 410 GHz for a dust polarization fraction $p = 0.1$. The 150 GHz channel is CMB dominated, while the 410 GHz channel is dust dominated. The 250 GHz channel provides information about the dust spectral index.

The first set of maps—the lensed CMB realizations—were obtained starting from the unlensed fiducial power spectrum C_ℓ^{XY} , from which Gaussian realizations of the CMB polarization were generated, which were then lensed by remapping the pixels by the deflection field. The deflection field is in turn derived from a Gaussian realization of the projected potential power spectrum $C_\ell^{\phi\phi}$; we neglect the effect of the integrated Sachs-Wolfe effect induced correlation $C_\ell^{X\phi}$. We have chosen our pixel size to be small compared to the RMS of the deflection angles ($\sim 2'$) so that errors due to interpolation back onto the regular grid after remapping are small. We have checked that the E and B -mode power spectra of these simulated lensed maps reproduces the lensed power spectra obtained from CAMB to within a few percent accuracy for the E -mode spectrum and to within five percent accuracy for the B -mode spectrum. While this is less accurate than the all-sky lensing simulations now performed by several groups using various interpolation schemes [45] [46] [47] [4], we believe that our flat-sky simulations are sufficiently accurate for our dust foreground study.

The second set of maps—the unlensed CMB realizations—were obtained from Gaussian realizations of the lensed fiducial power spectrum, \tilde{C}_ℓ^{XY} . These maps have the same power spectrum as the lensed CMB realizations, but have none of the lensing-induced non-Gaussianity.

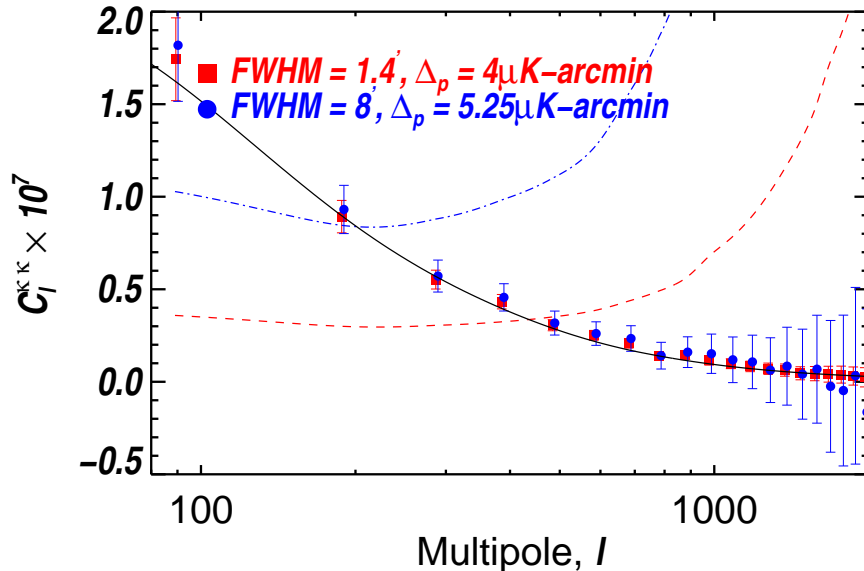


Figure 4. Validation of the EB quadratic estimator. The solid line is the power spectrum of the input convergence map $C_\ell^{\kappa\kappa}$, and the error bars show the estimated convergence power spectra averaged over 100 simulations. The dash curves are the lensing noise spectrum, $N_\ell^{\kappa,XY}$, for the two sets of survey parameters assumed.

Since the power spectrum of the convergence reconstructed on unlensed CMB maps is same as the lensing noise power spectrum predicted analytically from Eq. (2.11), these maps have been used for checking the accuracy and implementation details of the convergence and power spectrum estimators, as well as the testing effect of mask apodization.

Finally the CMB maps are scaled to antenna temperature units in the three bands at 150, 250 and 410 GHz, smoothed with an $8'$ beam, and uncorrelated Gaussian white noise is added to each pixel. The Stokes Q parameter of an example simulation is shown in Figure 3.

4 Results

This section describes our results in which we calculate the level of lensing bias that is expected from our dust polarization model. Finding a dust bias to be present, we apply the parametric multi-frequency foreground cleaning technique [23] described in Section 2.2, and establish a requirement for the accuracy with which the dust spectral index must be constrained in order to guarantee dust cleaning.

4.1 Foreground-free case

Before reporting the effect of the dust, we first demonstrate our reconstruction of the convergence from the EB quadratic estimator, using modes in the range $100 < \ell < 3000$, under the most idealized foreground-free case. Figure 4 shows the convergence power spectrum for our simulated 150 GHz channel with $5.25 \mu\text{K-arcmin}$ sensitivity and $8'$ angular resolution, as well as for a survey with $4 \mu\text{K-arcmin}$ sensitivity and $1.4'$ angular resolution similar to the planned ‘ACTPol Deep’ survey of [19]. The power spectrum estimates shown are the average

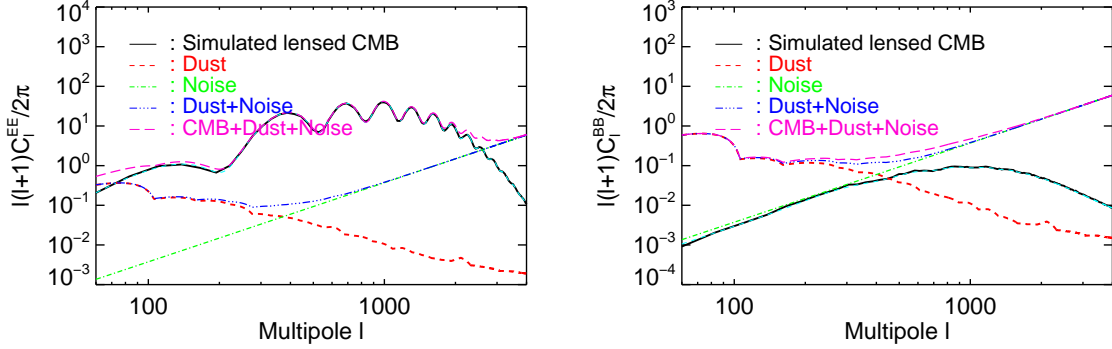


Figure 5. The lensed CMB E -mode (left panel) and B -mode (right panel) power spectrum is compared to the power spectrum of the dust ($p = 0.1$) and instrumental noise at 150 GHz. For comparison the fiducial E and B -mode power spectra is also shown (cyan).

over 100 simulations of $\hat{C}_\ell^{\kappa\kappa} - N_\ell^{\kappa,XY}$, while the corresponding error bar is given by

$$\Delta C_\ell^{\kappa\kappa} = \frac{\hat{C}_\ell^{\kappa\kappa} + N_\ell^{\kappa,XY}}{\sqrt{\ell \Delta \ell f_{\text{sky}}}}, \quad (4.1)$$

where we have applied a binning scheme $\Delta l = 98$ (thirty bins between $\ell = 40$ and $\ell = 3000$). The power spectrum estimates shown in Figure 4 represent an end to end validation of our CMB simulations, EB quadratic estimator, and power spectrum estimation pipeline.

4.2 Dust polarization bias at 150 GHz

To first assess the size of the dust contamination on the patch we are considering, we estimated the power spectrum of the simulated dust at 150 GHz and compared it to E and B -mode signal and noise power spectra, as shown in Figure 5 for the example of $p = 0.1$. For our dust model and choice of patch, the E and B -mode power spectra of the dust approximately follow a powerlaw given by $C_\ell^{\text{dust}} = (A \times p)^2 \ell^\beta$, where p is the polarization fraction, $A \simeq 120 \mu\text{K}$ and $\beta \simeq -3.5$. Our previous study [32] has shown that polarized dust at this level of power must be modeled and subtracted in order to derive unbiased estimates of the inflationary B -mode spectrum, a cosmological signal which is accessible in the $\ell < 200$ range of the B -mode power spectrum. The main question we seek to address in this study is whether this level of anisotropy power of foreground contamination is large enough to also bias the estimates of the lensing signal.

We have calculated the power spectrum of the convergence field reconstructed with the EB quadratic estimator using the dust contaminated 150 GHz channel, and show our results in Figure 6 for three different polarization fractions of $p = [0.01, 0.036, 0.1]$. We find that if the dust contamination is ignored during the lensing estimation, then a ‘dust noise bias’ dominates over the lensing power spectrum estimates for both the $p = 0.036$ and $p = 0.1$ case, but can be ignored for the $p = 0.01$ case.

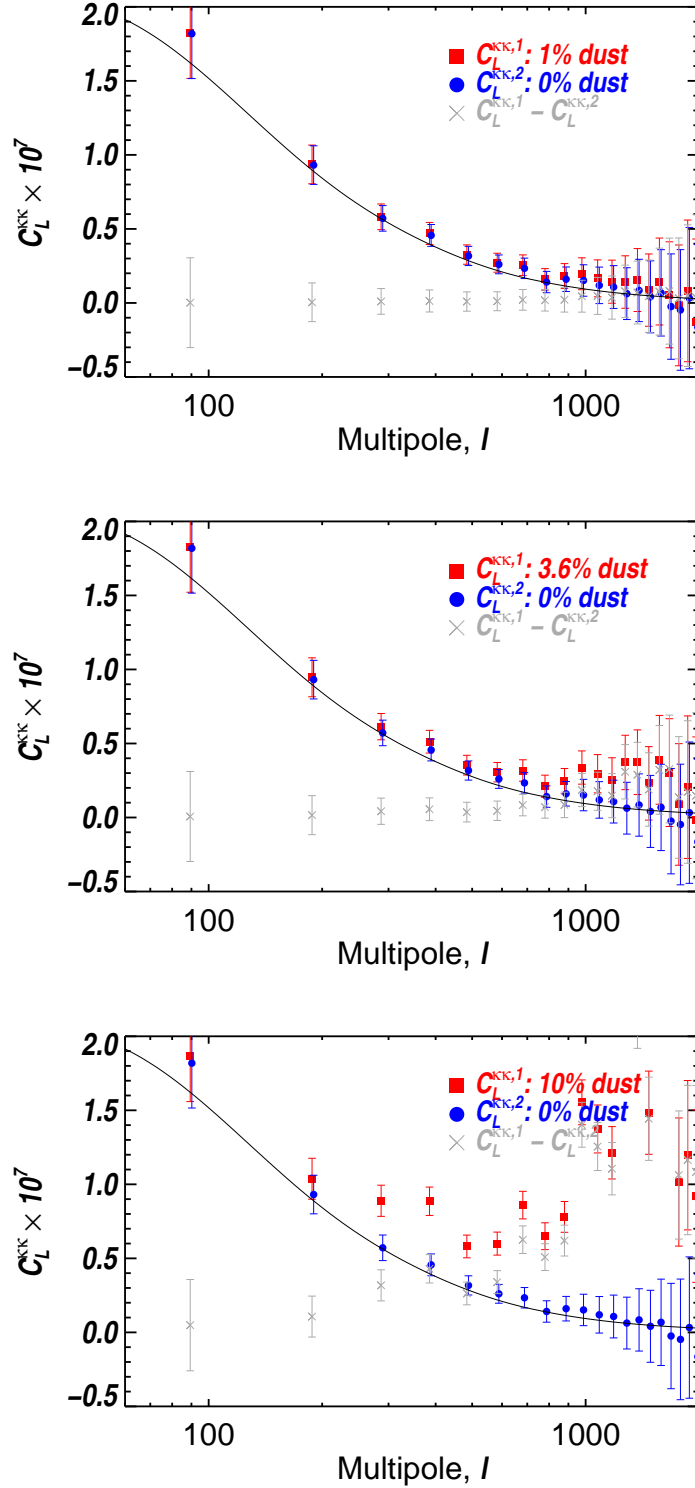


Figure 6. Effect of polarized dust at 150 GHz for surveys with sensitivity $\Delta_p = 5.25 \mu K - \text{arcmin}$. The upper, middle and lower panels show cases with dust polarization fractions of $p = 0.001, 0.036$ and 0.1 respectively. We find that for our dust model and choice of patch, diffuse polarized dust is expected to be a significant source of bias to C_ℓ^{KK} if the dust polarization fraction is greater than around 1 percent.

Although our demonstration of the dust bias will be dependent on the choice of patch we have assumed, and on the details of our polarized dust model and its power spectrum, we nonetheless conclude that diffuse polarized dust may in principle be a source of bias for future sub-orbital CMB surveys aiming at lensing estimates using the EB estimator, and that methods for foreground debiasing must therefore be developed.

For our dust model and choice of patch we can now roughly estimate that the requirement on the ‘dust suppression factor’ (the factor by which the polarized dust must be reduced at 150 GHz) is approximately (p_{crit}/p) , where we have estimated that the ‘critical polarization fraction’ p_{crit} , below which the effect of dust contamination becomes small compared to the noise level in the convergence power spectrum estimates, is approximately $p_{\text{crit}} = 0.01$. This requirement on the dust suppression factor, (p_{crit}/p) , will in turn set the requirement with which the dust spectral index must be estimated, which we will calculate in the next section.

4.3 Debiasing the effect of dust via foreground cleaning

Having established that our polarized dust model is leading to a bias in the lensing power spectrum, our main aims are 1) To test the multi-frequency foreground cleaning technique described in Section 2.2, in which the dust spectral index is first estimated from the data using the profile likelihood Eq. (2.15), before applying a linear least-squares component separation of the CMB and dust using Eq. (2.16) and propagation of the noise covariance using Eq. (2.17), and 2) To put requirements on the accuracy with which the dust spectral index must be estimated in order to guarantee dust cleaning.

For the homogeneous noise case that we have simulated, the final least squares combination of the data is a linear combination of the channel maps. However, the profile likelihood is a non-linear method involving quadratic combinations of the data, and so we have therefore numerically investigated its accuracy in determining the dust spectral index by carrying out 100 spectral index estimation and component separation simulations, each with a different CMB and noise realization.

Table 1 summarizes our results for our dust spectral index estimation simulations, for three cases $p = [0.036, 0.05, 0.1]$. First, we find that the greater the dust signal, the more accurately the dust spectral index can be estimated from the data. This is qualitatively consistent with the analysis of the profile likelihood of [48] in which increased dust contrast is shown to improve the accuracy of the dust spectral index estimation. We have also found that the profile likelihood returns an unbiased estimate for the dust spectral β when considering the average value obtained over the ensemble of CMB+noise realizations that we have analysed, but we also find that the profile likelihood width for any single noise underestimates the dust spectral index uncertainty. This breakdown of the profile likelihood appears to be related to the relatively low contrast regime of the polarization data we have simulated: If the dust intensity data is assumed to have the same frequency scaling as the polarization data, then the dust spectral index is first estimated with much higher accuracy, and the profile likelihood width and Monte Carlo average of the spectral index estimates agree well. This implies that any application of the profile likelihood to data should be accompanied by Monte Carlo simulations, given a Galactic foreground model, in order to more accurately quantify the spectral index uncertainty.

For each of the 100 spectral index estimates, we calculate the Z -matrix defined in Eq. (2.18); We will focus on the $Z_{\text{CMB,Dust}}$ matrix element, since this will quantify the fraction of dust that remains unsubtracted from the CMB component after the least squares

$(\beta_{\text{input}} = 1.65)$

p	β	$\Delta\beta$
0.036	1.69	0.43 (0.04)
0.05	1.67	0.22 (0.03)
0.1	1.66	0.06 (0.02)

Table 1. Mean and RMS of the dust spectral index estimate β , estimated from 100 component separation simulations varying CMB and noise realizations, for the three dust polarization fraction cases assumed; The values in parentheses are the mean value of the profile likelihood width. We find that spectral index uncertainty for any single noise realisation (shown in parentheses) is underestimated by the profile likelihood in the dust contrast regime of our polarization simulations.

$p = 0.036$		
Input:	CMB	Dust
Output:		
CMB	1	-0.06 ± 0.79
Dust	0	1.04 ± 0.41
$p = 0.05$		
Input:	CMB	Dust
Output:		
CMB	1	-0.01 ± 0.41
Dust	0	1.01 ± 0.21
$p = 0.1$		
Input:	CMB	Dust
Output:		
CMB	1	0.00 ± 0.10
Dust	0	1.00 ± 0.05

Table 2. Z -matrices, Eq. (2.18), averaged over 100 component separation simulations varying CMB and noise realizations, for three different dust polarization cases. The $Z_{\text{CMB,Dust}}$ matrix element quantifies the fraction of dust at 150 GHz that is mixed into the CMB after component separation, and so can be thought of as a ‘dust suppression factor’. We find that in the $p = 0.1$ case, the dust spectral index is estimated with enough accuracy to guarantee dust cleaning ($|\langle Z_{\text{CMB,Dust}} \rangle| \ll 1$), while for the $p = 0.36$ case dust cleaning is not guaranteed.

component separation. Table 2 gives the mean and RMS of Z -matrices for the three polarization fraction cases $p = [0.036, 0.05, 0.1]$. The basic conclusion is that while in the case of $p = 0.1$ the dust spectral index is always estimated accurately enough to guarantee dust cleaning ($\langle Z_{\text{CMB,Dust}} \rangle = 0.00 \pm 0.10$), in the case of $p = 0.036$ the dust is no longer bright enough to allow sufficiently accurate spectral index estimation, and for many simulations, there is an *amplification* of the dust contamination ($|Z_{\text{CMB,Dust}}| > 1$).

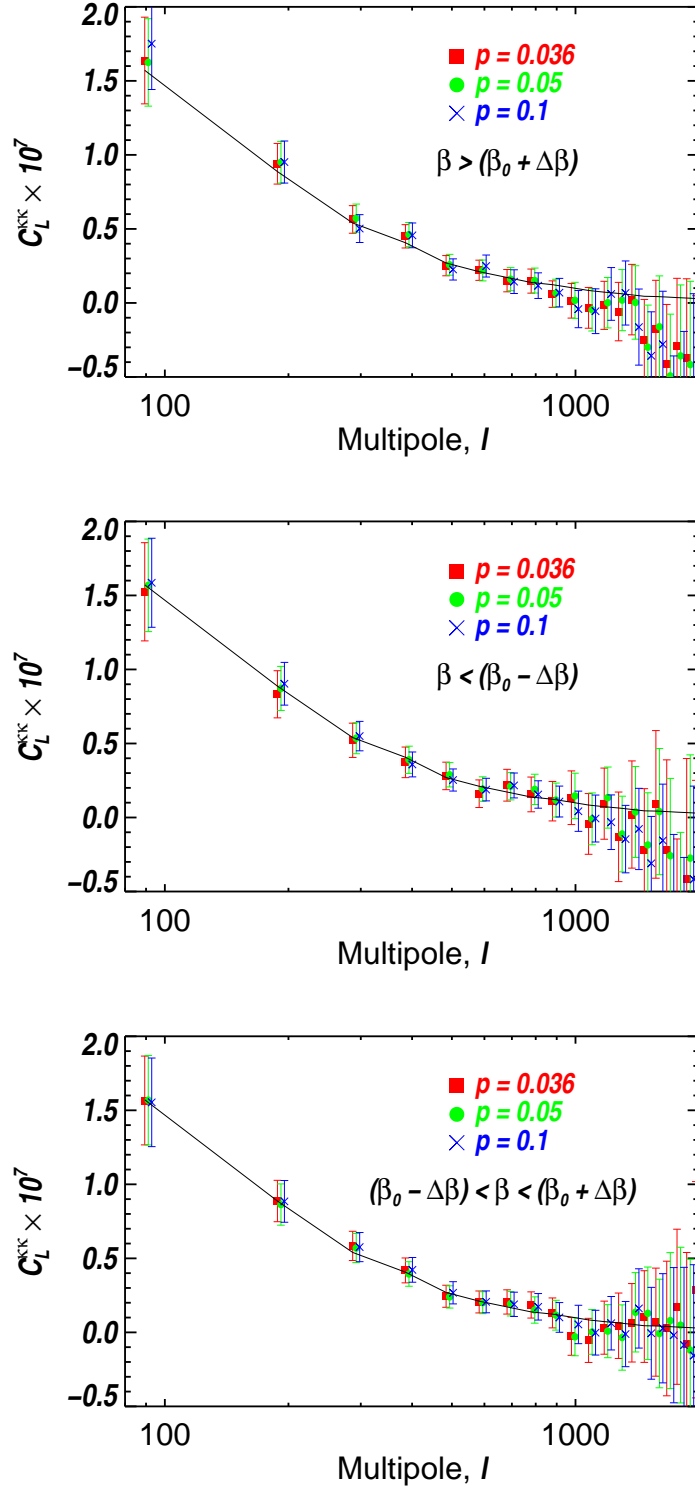


Figure 7. Convergence power spectrum of the estimated CMB component. The upper and middle panels shows the average convergence power spectrum for realisations with spectral index $\beta > [1.81, 1.76, 1.71]$ and $\beta < [1.49, 1.54, 1.59]$, respectively, for the three dust polarization fraction cases of $p = [0.036, 0.05, 0.1]$. The lower panel shows the average convergence power spectrum for those CMB components whose spectral index meets the accuracy requirement given in Eq. (4.2).

It therefore becomes important to be able to put a requirement on the accuracy, $\Delta\beta$, with which the dust spectral index must be estimated in order to guarantee foreground cleaning. This requirement can then either guide the application of our parametric component separation technique, or inform the usage of possible external spectral index prior information. For our case study we suggest the criterion

$$\Delta\beta < \left(\frac{p_{\text{crit}}}{p}\right) \times \left.\frac{\partial\beta}{\partial Z}\right|_{\beta_0}, \quad (4.2)$$

where we conservatively assume $p_{\text{crit}} = 0.01$; More generally, the factor (p_{crit}/p) can be thought of as the desired dust suppression factor for a given patch of sky. Qualitatively, there is therefore a requirement for greater spectral index precision for larger values of p . Quantitatively, we have numerically calculated $\left.\frac{\partial\beta}{\partial Z}\right|_{\beta_0} = 0.56$ from the function $Z(\beta)$, and so for the three cases $p = [0.036, 0.05, 0.1]$ we require $\Delta\beta < [0.16, 0.11, 0.06]$ respectively. We have checked that enforcement of this spectral index accuracy requirement leads to satisfactory dust cleaning. Figure 7 shows the average convergence power spectrum of the estimated CMB component for those realizations whose spectral index estimate meet this accuracy requirement (for instance those with $\beta = 1.65 \pm 0.06$ for the $p = 0.1$ case), for which we find satisfactorily debiased convergence power spectrum estimates after component separation. Conversely, the realizations with estimated dust spectral indices falling outside the required range show a biased convergence power spectrum after component separation.

5 Conclusions

Several ongoing and planned CMB polarization experiments are aiming to measure and characterise the lensing of the cosmic microwave background, in order to improve constraints on the parameters of the cosmological model. Within this context we have made the first specific study of the possible effect of diffuse polarized dust emission on the accuracy of the reconstruction of the lensing convergence signal. Our particular focus has been on performing a case study of a three channel balloon-borne CMB experiment covering the frequency range 150–410 GHz. Our numerical investigation is based on a dust polarization simulation and a flat-sky implementation of the Hu and Okamoto quadratic estimator. We found that for the sky patch under consideration, which is near to the region of sky that will be targeted by the EBEX experiment, and for plausible dust polarization fractions in the range 3.6–10%, the anisotropy of the diffuse dust polarization will be large enough at 150 GHz to bias the reconstruction of the convergence. Thus a multi-frequency experimental approach is imperative, and appropriate analysis methods must be developed for debiasing the effect of polarized dust.

In order to mitigate the effect of the dust and to debias the convergence power spectrum, we demonstrated a multi-frequency component separation technique in which the dust spectral index is first estimated from the data using a profile likelihood technique, before applying a least squares component separation. We found evidence for a dust contrast regime in which the accuracy of profile likelihood breaks down, both underestimating the spectral index uncertainty as well as providing spectral index estimates that are insufficiently accurate to guarantee dust cleaning. This highlights the possible need for external constraints on the frequency scaling of the polarized dust which can then be used as a prior, to stabilize the dust spectral index estimates to the accuracy required for sufficient dust cleaning. We proposed a

criterion, Eq. (4.2), which sets a requirement for the accuracy with which the spectral index of the foregrounds must be estimated in order to guarantee a given dust suppression factor. We then demonstrated that satisfactory dust cleaning was achieved for the cases in which the estimated spectral index met this requirement.

Acknowledgments

APSY acknowledges support from NASA grant number NNX08AG40G. Part of this work was supported by the PD51 INFN Grant. We acknowledge the use of the HEALPIX [49] and CAMB [44] packages.

References

- [1] A. Lewis and A. Challinor, *Weak gravitational lensing of the CMB*, *Phys. Rep.* **429** (June, 2006) 1–65, [[astro-ph/](#)].
- [2] R. Stompor and G. Efstathiou, *Gravitational lensing of cosmic microwave background anisotropies and cosmological parameter estimation*, *MNRAS* **302** (Feb., 1999) 735–747, [[astro-ph/](#)].
- [3] L. Perotto, J. Lesgourgues, S. Hannestad, H. Tu, and Y. Y Y Wong, *Probing cosmological parameters with the CMB: forecasts from Monte Carlo simulations*, *Journal of Cosmology and Astro-Particle Physics* **10** (Oct., 2006) 13–+, [[astro-ph/](#)].
- [4] A. Benoit-Lévy, K. M. Smith, and W. Hu, *Non-Gaussian structure of the lensed CMB power spectra covariance matrix*, *ArXiv e-prints* (May, 2012) [[arXiv:1205.0474](#)].
- [5] K. M. Smith, O. Zahn, and O. Doré, *Detection of gravitational lensing in the cosmic microwave background*, *Phys. Rev. D.* **76** (Aug., 2007) 043510, [[arXiv:0705.3980](#)].
- [6] S. Das, B. D. Sherwin, P. Aguirre, J. W. Appel, J. R. Bond, C. S. Carvalho, M. J. Devlin, J. Dunkley, R. Dünner, T. Essinger-Hileman, J. W. Fowler, A. Hajian, M. Halpern, M. Hasselfield, A. D. Hincks, R. Hlozek, K. M. Huffenberger, J. P. Hughes, K. D. Irwin, J. Klein, A. Kosowsky, R. H. Lupton, T. A. Marriage, D. Marsden, F. Menanteau, K. Moodley, M. D. Niemack, M. R. Nolta, L. A. Page, L. Parker, E. D. Reese, B. L. Schmitt, N. Sehgal, J. Sievers, D. N. Spergel, S. T. Staggs, D. S. Swetz, E. R. Switzer, R. Thornton, K. Visnjic, and E. Wollack, *Detection of the Power Spectrum of Cosmic Microwave Background Lensing by the Atacama Cosmology Telescope*, *Physical Review Letters* **107** (July, 2011) 021301, [[arXiv:1103.2124](#)].
- [7] A. van Engelen, R. Keisler, O. Zahn, K. A. Aird, B. A. Benson, L. E. Bleem, J. E. Carlstrom, C. L. Chang, H. M. Cho, T. M. Crawford, A. T. Crites, T. de Haan, M. A. Dobbs, J. Dudley, E. M. George, N. W. Halverson, G. P. Holder, W. L. Holzapfel, S. Hoover, Z. Hou, J. D. Hrubes, M. Joy, L. Knox, A. T. Lee, E. M. Leitch, M. Lueker, D. Luong-Van, J. J. McMahon, J. Mehl, S. S. Meyer, M. Millea, J. J. Mohr, T. E. Montroy, T. Natoli, S. Padin, T. Plagge, C. Pryke, C. L. Reichardt, J. E. Ruhl, J. T. Sayre, K. K. Schaffer, L. Shaw, E. Shirokoff, H. G. Spieler, Z. Staniszewski, A. A. Stark, K. Story, K. Vanderlinde, J. D. Vieira, and R. Williamson, *A measurement of gravitational lensing of the microwave background using South Pole Telescope data*, *ArXiv e-prints* (Feb., 2012) [[arXiv:1202.0546](#)].
- [8] L. E. Bleem, A. van Engelen, G. P. Holder, K. A. Aird, R. Armstrong, M. L. N. Ashby, M. R. Becker, B. A. Benson, T. Biesiadzinski, M. Brodwin, M. T. Busha, J. E. Carlstrom, C. L. Chang, H. M. Cho, T. M. Crawford, A. T. Crites, T. de Haan, S. Desai, M. A. Dobbs, O. Doré, J. Dudley, J. E. Geach, E. M. George, M. D. Gladders, A. H. Gonzalez, N. W. Halverson, N. Harrington, F. W. High, B. P. Holden, W. L. Holzapfel, S. Hoover, J. D. Hrubes, M. Joy, R. Keisler, L. Knox, A. T. Lee, E. M. Leitch, M. Lueker, D. Luong-Van, D. P. Marrone,

- J. Martinez-Manso, J. J. McMahon, J. Mehl, S. S. Meyer, J. J. Mohr, T. E. Montroy, T. Natoli, S. Padin, T. Plagge, C. Pryke, C. L. Reichardt, A. Rest, J. E. Ruhl, B. R. Saliwanchik, J. T. Sayre, K. K. Schaffer, L. Shaw, E. Shirokoff, H. G. Spieler, B. Stalder, S. A. Stanford, Z. Staniszewski, A. A. Stark, D. Stern, K. Story, A. Vallinotto, K. Vanderlinde, J. D. Vieira, R. H. Wechsler, R. Williamson, and O. Zahn, *A Measurement of the Correlation of Galaxy Surveys with CMB Lensing Convergence Maps from the South Pole Telescope*, *ArXiv e-prints* (Mar., 2012) [[arXiv:1203.4808](#)].
- [9] B. D. Sherwin, J. Dunkley, S. Das, J. W. Appel, J. R. Bond, C. S. Carvalho, M. J. Devlin, R. Dünner, T. Essinger-Hileman, J. W. Fowler, A. Hajian, M. Halpern, M. Hasselfield, A. D. Hincks, R. Hlozek, J. P. Hughes, K. D. Irwin, J. Klein, A. Kosowsky, T. A. Marriage, D. Marsden, K. Moodley, F. Menanteau, M. D. Niemack, M. R. Nolta, L. A. Page, L. Parker, E. D. Reese, B. L. Schmitt, N. Sehgal, J. Sievers, D. N. Spergel, S. T. Staggs, D. S. Swetz, E. R. Switzer, R. Thornton, K. Visnjic, and E. Wollack, *Evidence for Dark Energy from the Cosmic Microwave Background Alone Using the Atacama Cosmology Telescope Lensing Measurements*, *Physical Review Letters* **107** (July, 2011) 021302, [[arXiv:1105.0419](#)].
- [10] L. Perotto, J. Bobin, S. Plaszczynski, J.-L. Starck, and A. Lavabre, *Reconstruction of the cosmic microwave background lensing for Planck*, *A&A* **519** (Sept., 2010) A4.
- [11] D. Hanson, A. Challinor, G. Efstathiou, and P. Bielewicz, *CMB temperature lensing power reconstruction*, *Phys. Rev. D.* **83** (Feb., 2011) 043005, [[arXiv:1008.4403](#)].
- [12] W. Hu and T. Okamoto, *Mass Reconstruction with Cosmic Microwave Background Polarization*, *ApJ* **574** (Aug., 2002) 566–574, [[astro-ph/](#)].
- [13] M. Kesden, A. Cooray, and M. Kamionkowski, *Lensing reconstruction with CMB temperature and polarization*, *Phys. Rev. D.* **67** (June, 2003) 123507, [[astro-ph/](#)].
- [14] D. Hanson, G. Rocha, and K. Górski, *Lensing reconstruction from Planck sky maps: inhomogeneous noise*, *MNRAS* **400** (Dec., 2009) 2169–2173, [[arXiv:0907.1927](#)].
- [15] N. J. Miller, M. Shimon, and B. G. Keating, *CMB beam systematics: Impact on lensing parameter estimation*, *Phys. Rev. D.* **79** (Mar., 2009) 063008, [[arXiv:0806.3096](#)].
- [16] M. Su, A. P. S. Yadav, and M. Zaldarriaga, *Impact of instrumental systematic contamination on the lensing mass reconstruction using the CMB polarization*, *Phys. Rev. D.* **79** (June, 2009) 123002, [[arXiv:0901.0285](#)].
- [17] A. Amblard, C. Vale, and M. White, *Weak lensing of the CMB by large-scale structure*, *New A* **9** (Oct., 2004) 687–704, [[astro-ph/](#)].
- [18] K. M. Smith, A. Cooray, S. Das, O. Doré, D. Hanson, C. Hirata, M. Kaplinghat, B. Keating, M. Loverde, N. Miller, G. Rocha, M. Shimon, and O. Zahn, *Gravitational Lensing*, in *American Institute of Physics Conference Series* (S. Dodelson, D. Baumann, A. Cooray, J. Dunkley, A. Fraisse, M. G. Jackson, A. Kogut, L. Krauss, M. Zaldarriaga, & K. Smith, ed.), vol. 1141 of *American Institute of Physics Conference Series*, pp. 121–178, June, 2009. [arXiv:0811.3916](#).
- [19] M. D. Niemack, P. A. R. Ade, J. Aguirre, F. Barrientos, J. A. Beall, J. R. Bond, J. Britton, H. M. Cho, S. Das, M. J. Devlin, S. Dicker, J. Dunkley, R. Dünner, J. W. Fowler, A. Hajian, M. Halpern, M. Hasselfield, G. C. Hilton, M. Hilton, J. Hubmayr, J. P. Hughes, L. Infante, K. D. Irwin, N. Jarosik, J. Klein, A. Kosowsky, T. A. Marriage, J. McMahon, F. Menanteau, K. Moodley, J. P. Nibarger, M. R. Nolta, L. A. Page, B. Partridge, E. D. Reese, J. Sievers, D. N. Spergel, S. T. Staggs, R. Thornton, C. Tucker, E. Wollack, and K. W. Yoon, *ACTPol: a polarization-sensitive receiver for the Atacama Cosmology Telescope*, in *Society of Photo-Optical Instrumentation Engineers (SPIE) Conference Series*, vol. 7741 of *Society of Photo-Optical Instrumentation Engineers (SPIE) Conference Series*, July, 2010. [arXiv:1006.5049](#).
- [20] J. J. McMahon, K. A. Aird, B. A. Benson, L. E. Bleem, J. Britton, J. E. Carlstrom, C. L. Chang, H. S. Cho, T. de Haan, T. M. Crawford, A. T. Crites, A. Datesman, M. A. Dobbs,

- W. Everett, N. W. Halverson, G. P. Holder, W. L. Holzapfel, D. Hrubes, K. D. Irwin, M. Joy, R. Keisler, T. M. Lanting, A. T. Lee, E. M. Leitch, A. Loehr, M. Lueker, J. Mehl, S. S. Meyer, J. J. Mohr, T. E. Montroy, M. D. Niemack, C. C. Ngeow, V. Novosad, S. Padin, T. Plagge, C. Pryke, C. Reichardt, J. E. Ruhl, K. K. Schaffer, L. Shaw, E. Shirokoff, H. G. Spieler, B. Stadler, A. A. Stark, Z. Staniszewski, K. Vanderlinde, J. D. Vieira, G. Wang, R. Williamson, V. Yefremenko, K. W. Yoon, O. Zhan, and A. Zenteno, *SPTpol: an instrument for CMB polarization*, in *American Institute of Physics Conference Series* (B. Young, B. Cabrera, & A. Miller, ed.), vol. 1185 of *American Institute of Physics Conference Series*, pp. 511–514, Dec., 2009.
- [21] B. Reichborn-Kjennerud, A. M. Aboobaker, P. Ade, F. Aubin, C. Baccigalupi, C. Bao, J. Borrill, C. Cantalupo, D. Chapman, J. Didier, M. Dobbs, J. Grain, W. Grainger, S. Hanany, and et al, *EBEX: a balloon-borne CMB polarization experiment*, in *Society of Photo-Optical Instrumentation Engineers (SPIE) Conference Series*, vol. 7741, July, 2010. [arXiv:1007.3672](#).
- [22] A. T. Lee, H. Tran, P. Ade, K. Arnold, J. Borrill, M. A. Dobbs, J. Errard, N. Halverson, W. L. Holzapfel, and et. al., *POLARBEAR: Ultra-high Energy Physics with Measurements of CMB Polarization*, in *American Institute of Physics Conference Series* (H. Kodama & K. Ioka, ed.), vol. 1040 of *American Institute of Physics Conference Series*, pp. 66–77, Aug., 2008.
- [23] R. Stompor, S. Leach, F. Stivoli, and C. Baccigalupi, *Maximum likelihood algorithm for parametric component separation in cosmic microwave background experiments*, *MNRAS* **392** (Jan., 2009) 216–232, [[arXiv:0804.2645](#)].
- [24] M. Zaldarriaga and U. Seljak, *Reconstructing Projected Matter Density from Cosmic Microwave Background*, [astro-ph/9810257](#).
- [25] W. Hu, *Weak lensing of the CMB: A harmonic approach*, *Phys. Rev. D.* **62** (Aug., 2000) 043007, [[astro-ph/](#)].
- [26] L. Knox, *Determination of inflationary observables by cosmic microwave background anisotropy experiments*, *Phys. Rev. D.* **52** (Oct., 1995) 4307–4318, [[astro-ph/](#)].
- [27] W. Hu, *The Angular Trispectrum of the CMB*, [astro-ph/0105117](#).
- [28] W. Hu, *Mapping the Dark Matter through the Cosmic Microwave Background Damping Tail*, *The Astrophysical Journal Letters* (Aug., 2001) L79+, [[astro-ph/0105424](#)].
- [29] W. Hu, S. DeDeo, and C. Vale, *Cluster mass estimators from CMB temperature and polarization lensing*, *New Journal of Physics* **9** (Dec., 2007) 441, [[astro-ph/](#)].
- [30] J. Yoo, M. Zaldarriaga, and L. Hernquist, *Lensing reconstruction of cluster-mass cross correlation with cosmic microwave background polarization*, *Phys. Rev. D.* **81** (June, 2010) 123006, [[arXiv:1005.0847](#)].
- [31] F. Stivoli, J. Grain, S. M. Leach, M. Tristram, C. Baccigalupi, and R. Stompor, *Maximum likelihood, parametric component separation and CMB B-mode detection in suborbital experiments*, *MNRAS* **408** (Nov., 2010) 2319–2335, [[arXiv:1004.4756](#)].
- [32] Y. Fantaye, F. Stivoli, J. Grain, S. M. Leach, M. Tristram, C. Baccigalupi, and R. Stompor, *Estimating the tensor-to-scalar ratio and the effect of residual foreground contamination*, *J. Cosmology Astropart. Phys.* **8** (Aug., 2011) 1, [[arXiv:1104.1367](#)].
- [33] T. E. Montroy, P. A. R. Ade, J. J. Bock, J. R. Bond, J. Borrill, A. Boscaleri, P. Cabella, C. R. Contaldi, B. P. Crill, P. de Bernardis, A. De Gasperis, G. and de Oliveira-Costa, and et. al., *A Measurement of the CMB $\langle EE \rangle$ Spectrum from the 2003 Flight of BOOMERANG*, *ApJ* **647** (Aug., 2006) 813–822, [[astro-ph/](#)].
- [34] M. L. Brown, P. Ade, J. Bock, M. Bowden, G. Cahill, P. G. Castro, S. Church, T. Culverhouse, R. B. Friedman, K. Ganga, W. K. Gear, S. Gupta, et. al., and The QUaD collaboration, *Improved Measurements of the Temperature and Polarization of the Cosmic Microwave Background from QUaD*, *ApJ* **705** (Nov., 2009) 978–999, [[arXiv:0906.1003](#)].

- [35] C. L. Reichardt, P. A. R. Ade, J. J. Bock, J. R. Bond, J. A. Brevik, C. R. Contaldi, M. D. Daub, J. T. Dempsey, and et. al., *High-Resolution CMB Power Spectrum from the Complete ACBAR Data Set*, *ApJ* **694** (Apr., 2009) 1200–1219, [[arXiv:0801.1491](#)].
- [36] QUIET Collaboration, C. Bischoff, A. Brizius, I. Buder, Y. Chinone, K. Cleary, R. N. Dumoulin, A. Kusaka, R. Monsalve, S. K. Næss, L. B. Newburgh, R. Reeves, K. M. Smith, I. K. Wehus, J. A. Zuntz, J. T. L. Zwart, L. Bronfman, R. Bustos, S. E. Church, C. Dickinson, H. K. Eriksen, P. G. Ferreira, T. Gaier, J. O. Gundersen, M. Hasegawa, M. Hazumi, K. M. Huffenberger, M. E. Jones, P. Kangaslahti, D. J. Kapner, C. R. Lawrence, M. Limon, J. May, J. J. McMahon, A. D. Miller, H. Nguyen, G. W. Nixon, T. J. Pearson, L. Piccirillo, S. J. E. Radford, A. C. S. Readhead, J. L. Richards, D. Samtleben, M. Seiffert, M. C. Shepherd, S. T. Staggs, O. Tajima, K. L. Thompson, K. Vanderlinde, R. Williamson, and B. Winstein, *First Season QUIET Observations: Measurements of Cosmic Microwave Background Polarization Power Spectra at 43 GHz in the Multipole Range $25 < l < 475$* , *ApJ* **741** (Nov., 2011) 111, [[arXiv:1012.3191](#)].
- [37] R. Keisler, C. L. Reichardt, K. A. Aird, B. A. Benson, L. E. Bleem, J. E. Carlstrom, C. L. Chang, H. M. Cho, T. M. Crawford, A. T. Crites, T. de Haan, M. A. Dobbs, J. Dudley, E. M. George, N. W. Halverson, G. P. Holder, W. L. Holzapfel, S. Hoover, Z. Hou, J. D. Hrubes, M. Joy, L. Knox, A. T. Lee, E. M. Leitch, M. Lueker, D. Luong-Van, J. J. McMahon, J. Mehl, S. S. Meyer, M. Millea, J. J. Mohr, T. E. Montroy, T. Natoli, S. Padin, T. Plagge, C. Pryke, J. E. Ruhl, K. K. Schaffer, L. Shaw, E. Shirokoff, H. G. Spieler, Z. Staniszewski, A. A. Stark, K. Story, A. van Engelen, K. Vanderlinde, J. D. Vieira, R. Williamson, and O. Zahn, *A Measurement of the Damping Tail of the Cosmic Microwave Background Power Spectrum with the South Pole Telescope*, *ApJ* **743** (Dec., 2011) 28, [[arXiv:1105.3182](#)].
- [38] D. J. Schlegel, D. P. Finkbeiner, and M. Davis, *Maps of Dust Infrared Emission for Use in Estimation of Reddening and Cosmic Microwave Background Radiation Foregrounds*, *ApJ* **500** (June, 1998) 525–+, [[astro-ph/](#)].
- [39] WMAP Collaboration, L. Page et al., *Three year Wilkinson Microwave Anisotropy Probe (WMAP) observations: Polarization analysis*, *Astrophys. J. Suppl.* **170** (2007) 335, [[astro-ph/0603450](#)].
- [40] G. Giardino, A. J. Banday, K. M. Górski, K. Bennett, J. L. Jonas, and J. Tauber, *Towards a model of full-sky Galactic synchrotron intensity and linear polarisation: A re-analysis of the Parkes data*, *A&A* **387** (May, 2002) 82–97, [[astro-ph/](#)].
- [41] A. Kogut, J. Dunkley, C. L. Bennett, O. Doré, B. Gold, M. Halpern, G. Hinshaw, N. Jarosik, E. Komatsu, M. R. Nolta, N. Odegard, L. Page, D. N. Spergel, G. S. Tucker, J. L. Weiland, E. Wollack, and E. L. Wright, *Three-Year Wilkinson Microwave Anisotropy Probe (WMAP) Observations: Foreground Polarization*, *ApJ* **665** (Aug., 2007) 355–362, [[arXiv:0704.3991](#)].
- [42] A. Benoît, P. Ade, A. Amblard, R. Ansari, É. Aubourg, S. Bargout, J. G. Bartlett, J.-P. Bernard, R. S. Bhatia, A. Blanchard, J. J. Bock, A. Boscaleri, F. R. Bouchet, A. Bourrachot, P. Camus, F. Couchot, P. de Bernardis, J. Delabrouille, F.-X. Désert, O. Doré, M. Douspis, L. Dumoulin, X. Dupac, P. Filliatre, P. Fosalba, K. Ganga, F. Gannaway, B. Gautier, M. Giard, Y. Giraud-Héraud, R. Gispert, L. Guglielmi, J.-C. Hamilton, S. Hanany, S. Henrot-Versillé, J. Kaplan, G. Lagache, J.-M. Lamarre, A. E. Lange, J. F. Macías-Pérez, K. Madet, B. Maffei, C. Magneville, D. P. Marrone, S. Masi, F. Mayet, A. Murphy, F. Naraghi, F. Nati, G. Patanchon, G. Perrin, M. Piat, N. Ponthieu, S. Prunet, J.-L. Puget, C. Renault, C. Rosset, D. Santos, A. Starobinsky, I. Strukov, R. V. Sudiwala, R. Teyssier, M. Tristram, C. Tucker, J.-C. Vanel, D. Vibert, E. Wakui, and D. Yvon, *First detection of polarization of the submillimetre diffuse galactic dust emission by Archeops*, *A&A* **424** (Sept., 2004) 571–582, [[astro-ph/](#)].
- [43] E. Komatsu, K. M. Smith, J. Dunkley, C. L. Bennett, B. Gold, G. Hinshaw, N. Jarosik, D. Larson, M. R. Nolta, L. Page, D. N. Spergel, M. Halpern, R. S. Hill, A. Kogut, M. Limon,

- S. S. Meyer, N. Odegard, G. S. Tucker, J. L. Weiland, E. Wollack, and E. L. Wright, *Seven-year Wilkinson Microwave Anisotropy Probe (WMAP) Observations: Cosmological Interpretation*, *ApJS* **192** (Feb., 2011) 18–+, [[arXiv:1001.4538](#)].
- [44] A. Lewis, A. Challinor, and A. Lasenby, *Efficient Computation of Cosmic Microwave Background Anisotropies in Closed Friedmann-Robertson-Walker Models*, *ApJ* **538** (Aug., 2000) 473–476, [[astro-ph/](#)].
- [45] A. Lewis, *Lensed CMB simulation and parameter estimation*, *Phys. Rev. D.* **71** (Apr., 2005) 083008–+, [[astro-ph/](#)].
- [46] S. Basak, S. Prunet, and K. Benabed, *Simulating weak lensing of CMB maps*, *A&A* **508** (Dec., 2009) 53–62.
- [47] G. Lavaux and B. D. Wandelt, *Fast and Optimal Cosmic Microwave Background Lensing Using Statistical Interpolation on the Sphere*, *ApJS* **191** (Nov., 2010) 32–42, [[arXiv:1003.4984](#)].
- [48] J. Errard, F. Stivoli, and R. Stompor, *Framework for performance forecasting and optimization of CMB B-mode observations in the presence of astrophysical foregrounds*, *Phys. Rev. D.* **84** (Sept., 2011) 063005.
- [49] K. M. Górski, E. Hivon, A. J. Banday, B. D. Wandelt, F. K. Hansen, M. Reinecke, and M. Bartelmann, *HEALPix: A Framework for High-Resolution Discretization and Fast Analysis of Data Distributed on the Sphere*, *ApJ* **622** (Apr., 2005) 759–771, [[astro-ph/](#)].